



**HAL**  
open science

## Emerging investigator series: photocatalysis for MBR effluent post-treatment: assessing the effects of effluent organic matter characteristics

Mostafa Maghsoodi, Céline Jacquin, Benoit Teychené, Marc Heran,  
Volodymyr Tarabara, Geoffroy Lesage, Samuel Snow

### ► To cite this version:

Mostafa Maghsoodi, Céline Jacquin, Benoit Teychené, Marc Heran, Volodymyr Tarabara, et al.. Emerging investigator series: photocatalysis for MBR effluent post-treatment: assessing the effects of effluent organic matter characteristics. *Environmental Science: Water Research and Technology*, 2019, 5 (3), pp.482-494. 10.1039/c8ew00734a . hal-03823748

**HAL Id: hal-03823748**

**<https://hal.umontpellier.fr/hal-03823748>**

Submitted on 21 Sep 2023

**HAL** is a multi-disciplinary open access archive for the deposit and dissemination of scientific research documents, whether they are published or not. The documents may come from teaching and research institutions in France or abroad, or from public or private research centers.

L'archive ouverte pluridisciplinaire **HAL**, est destinée au dépôt et à la diffusion de documents scientifiques de niveau recherche, publiés ou non, émanant des établissements d'enseignement et de recherche français ou étrangers, des laboratoires publics ou privés.

1 **Title: Photocatalysis for MBR Effluent Post-Treatment: Assessing the Effects of Effluent**  
2 **Organic Matter Characteristics**

3 Authors:

4 Mostafa Maghsoodi<sup>1T</sup>, Céline Jacquin<sup>2T</sup>, Benoit Teychené<sup>3</sup>, Marc Heran<sup>2</sup>, Volodymyr V. Tarabara<sup>4</sup>,  
5 Geoffroy Lesage<sup>\*2</sup>, Samuel D. Snow<sup>\*1</sup>

6 <sup>1</sup>Department of Civil and Environmental Engineering, Louisiana State University, 3255 Patrick Taylor  
7 Hall, Baton Rouge, Louisiana 70803, United States.

8 <sup>2</sup>IEM (Institut Européen des Membranes), UMR 5635 (CNRS-ENSCM-UM),  
9 Université de Montpellier, Place E. Bataillon, F- 34095, Montpellier, France.

10 <sup>3</sup>Institut de Chimie des Milieux et Matériaux de Poitiers (IC2MP – UMR CNRS 7285), Université de  
11 Poitiers, Ecole Nationale Supérieure d'Ingénieurs de Poitiers, 7 rue Marcel Doré, Bâtiment 16, TSA  
12 41105, 86073 Poitiers Cedex 9, France.

13 <sup>4</sup>Department of Civil and Environmental Engineering, Michigan State University, 428 S. Shaw Lane,  
14 East Lansing, Michigan 48824, United States.

15 <sup>T</sup>These authors contributed equally.

16 \*Corresponding authors: [SSnow@lsu.edu](mailto:SSnow@lsu.edu); [Geoffroy.Lesage@umontpellier.fr](mailto:Geoffroy.Lesage@umontpellier.fr);

17  
18 **Abstract:** Dissolved organic matter (DOM) poses a serious challenge to applied photocatalysis.  
19 Membranes may offer a promising synergistic opportunity to enable efficient photocatalysts in the  
20 presence of DOM. Membrane bioreactor (MBR) effluent from a municipal treatment plant was studied  
21 to elucidate the effects of filtration and organic matter composition on photocatalysis. Effluent  
22 samples were collected from MBR units during routine operation and before/after chemical cleaning.  
23 Additional DOM samples from the bulk supernatant were separated into colloidal, hydrophobic and  
24 transphilic fractions, providing a novel examination of the inhibition potential of DOM. These DOM  
25 fractions and the effluent organic matter (EfOM) samples were then characterized utilizing three-  
26 dimensional excitation–emission matrix (3DEEM) fluorescence spectroscopy and assayed for their  
27 potential to inhibit TiO<sub>2</sub>-mediated photocatalytic degradation of a probe compound, *para*-  
28 chlorobenzoic acid (*p*CBA). The colloidal fraction of DOM was found to exert the strongest

29 inhibition, followed by the transphilic, then the hydrophobic fractions; at 5 mgC/L, these fractions  
30 reduced the photodegradation rates by approximately 75%, 27%, and 17%, respectively. Of the  
31 effluent samples, EfOM from the recently-cleaned membrane caused the greatest inhibition of  
32 photocatalysis (~100% reduction at 0.5 to 2.0 mgC/L), whereas the effluent from the fouled membrane  
33 provided the least inhibition (~33% reduction at 2.0 mgC/L). The 3DEEM analysis predicted  
34 inhibitory action of both DOM and EfOM, based on total fluorescence volumes. Results here  
35 demonstrate the prospective utility of combining membrane technologies with photocatalytic  
36 processes.

37

## 38 **1. Introduction**

39 As the human population continues to grow, careful utilization of natural resources becomes  
40 increasingly more important. Water usage, and particularly reuse, is a critical topic for many  
41 communities.<sup>1,2</sup> The development of membrane bioreactor (MBR) technology has been an important  
42 step towards wastewater reuse, given substantial advantages over conventional activated sludge  
43 systems in terms of improved efficiency and effluent quality.<sup>3</sup> Despite these benefits that stem from  
44 the use a physical barrier (membranes), several types of contaminants can pass through the membranes  
45 and pose significant health risks upon release of the effluent into the environment. Indeed, viruses  
46 have been found in the effluents of state-of-the-art MBR treatment plants.<sup>4, 5</sup> In addition,  
47 pharmaceuticals<sup>6, 7</sup> and, more recently, antibiotic resistant genes have drawn attention as significant  
48 concerns posing environmental and health risks.<sup>8</sup> Thus, MBR systems require a disinfection step post-  
49 filtration to provide a safeguard. Although UV disinfection can be used in lieu of chlorination, and  
50 thereby avoid the necessity for an added dechlorination step, there are disadvantages: UV treatment  
51 does not significantly degrade antibiotic resistant genes<sup>8</sup> and many pollutants are recalcitrant to UV at  
52 commonly applied UV doses.<sup>9</sup>

53 Given these post-filtration challenges, an integration of innovative technologies could provide the key  
54 functionality to eliminate the remaining hazards from MBR effluent. In particular, photocatalytic  
55 materials applied in conjunction with existing UV dosing systems could produce reactive oxygen to

56 destroy these contaminants via advanced oxidation processes.<sup>9-12</sup> Germicidal UV radiation, a subset of  
57 the spectrum of short-wavelength UV light, often called UVC,<sup>13, 14</sup> can be enhanced by the addition of  
58 photocatalytic processes to promote the production of reactive oxygen species (ROS). These ROS are  
59 known to be particularly effective at inactivating viruses compared to bacteria which have protective  
60 cell membranes.<sup>15-18</sup> For example, the inactivation kinetics *Escherichia coli* by hydroxyl radicals  
61 ( $\cdot\text{OH}$ ) or by singlet oxygen ( $^1\text{O}_2$ ) have been shown to have a lag-phase where the cell membrane  
62 protects the bacteria's intracellular components against ROS attack,<sup>15, 16, 18</sup> whereas the genetic and  
63 essential components of viruses, such as MS2 bacteriophage, have very little protection and therefore  
64 no delay in their inactivation kinetics.<sup>15, 16</sup> A combined UVC-photocatalytic system is a plausible  
65 conception that could serve as an advanced oxidation process to oxidize pharmaceutical compounds in  
66 addition to providing disinfection activity.<sup>10</sup>

67 Application of photocatalytic processes to natural or waste waters faces a significant challenge in the  
68 form of non-target organic matter interferences. In the case of MBRs, effluent organic matter (EfOM)  
69 contains a variety of molecules that are known to quench hydroxyl radicals ( $\cdot\text{OH}$ ),<sup>19</sup> which are  
70 generally the most important ROS in any advanced oxidation—including  $\text{TiO}_2$  mediated  
71 photocatalysis. MBR EfOM is a complex mixture of organic molecules such as proteins,  
72 polysaccharides, humic substances and nucleic acids.<sup>20-23</sup> These molecules originate primarily from  
73 microbial activity (soluble microbial products, SMPs), produced during secondary biological treatment  
74 (via suspended or attached growth processes) , and are typically found at concentrations ranging from  
75 3 to 25 mgC/L.<sup>21, 22, 24-27</sup> EfOM can interfere with photocatalytic treatment through different inhibitory  
76 mechanisms. First, EfOM absorbs significant amounts of UV light, limiting the amount of photons  
77 available for catalyst excitation.<sup>28</sup> Second, EfOM quenches ROS, preventing reactions with the target  
78 compounds or microorganisms.<sup>29, 30</sup> This competition for ROS between the non-target EfOM and the  
79 target constituents can occur in two ways: scavenging of surface-bound ROS by EfOM and quenching  
80 of bulk phase ROS.<sup>15, 29, 31, 32</sup> Within the complex mixture of EfOM, less than 2% of the dissolved and  
81 colloidal organic materials are considered target contaminants, such as viruses or pharmaceuticals that  
82 originate from the influent wastewater;<sup>33</sup> thus, most photocatalytically generated  $\cdot\text{OH}$  radicals will be

83 quenched by reactions with non-target EfOM. Indeed, EfOM has been reported to scavenge between  
84 65 and 95% of  $\cdot\text{OH}$  in conventional effluents and is considered the most important  $\cdot\text{OH}$ -scavenger in  
85 such systems.<sup>34, 35</sup> EfOM constituents, such as fulvic acid and humic acid (HA), have a net negative  
86 charge above pH 3 due to the presence of phenolic and carboxylic groups.<sup>36, 37</sup> These molecules can  
87 therefore interact favorably with and adsorb onto the polar surface of  $\text{TiO}_2$ , reacting directly with ROS  
88 production sites.

89 It is important to understand the factors that control surface and bulk quenching mechanisms; ROS-  
90 EfOM reactivity and EfOM-photocatalyst adsorption affinities drive bulk and surface quenching  
91 routes, respectively. Different ROS have differential reactivities; for example, singlet oxygen ( $^1\text{O}_2$ ) is  
92 less reactive and more selective than  $\cdot\text{OH}$ .<sup>38</sup> Likewise, EfOM constituents may also vary in propensity  
93 to react with ROS, with some compounds being recalcitrant to strong oxidants, while others readily  
94 react with weaker ROS, such as  $^1\text{O}_2$ .<sup>30, 39</sup> With regard to adsorption interactions, the nature of the  
95 photocatalyst surface will determine the type of EfOM molecules that will adsorb onto the  
96 photocatalyst surface. These types of interactions have been studied in depth for the case of membrane  
97 fouling by organic matter,<sup>40-42</sup> and offer potential insights into DOM-photocatalyst interactions.

98 Membrane technology can be used to selectively remove fractions of organic matter. In the case of an  
99 MBR treating municipal wastewater, the membrane's material, pore size, and fouling state affect its  
100 selectivity and, therefore, the composition of the EfOM.<sup>43</sup> It is known that, in general, hydrophilic  
101 macromolecular and colloidal portions of organic matter cause more reversible membrane fouling than  
102 other fractions in MBR systems by forming a cake layer.<sup>41, 44, 45</sup> Fouling changes the effective pore size  
103 and surface characteristics of membranes; consequently, permeate quality changes over the operational  
104 timeline, since the last chemical cleaning event.<sup>46-48</sup> Membrane operation may control DOM retention  
105 and thereby the composition of DOM that passes through (EfOM); therefore, the time since last  
106 cleaning event could be an important parameter when considering the use of effluent disinfection  
107 strategies. The extent to which membrane operation time can be used as a control EfOM quality is not  
108 well known. A better understanding of the variability of EfOM constituents as a function of membrane  
109 operational parameters is critical for applying post-filtration disinfection technologies. Elucidating the

110 effects of membrane operation on EfOM content provides an excellent opportunity to scrutinize the  
111 effects of EfOM constituents on photocatalytic processes, a significant area of need for the field of  
112 photocatalytic water treatment.

113 While TiO<sub>2</sub> systems have been studied extensively, the mechanisms driving ROS inhibition by DOM  
114 are poorly understood. A recent literature review quantified the number of research articles  
115 investigating “photocatalysis” and “natural organic matter” and found that of the 17,500 papers found  
116 when searching for photocatalysis, only 0.8% (137) also referenced DOM.<sup>49</sup> The segregation of DOM  
117 into fractions to discern phenomenological effects of constituents on photocatalytic processes is  
118 therefore a critical step towards practical application of photocatalysts. A study completed in 2014 on  
119 the effects of size-fractionation of DOM on the photocatalytic degradation of DOM by TiO<sub>2</sub> is perhaps  
120 the first report to scrutinize the inhibitory mechanism by analyzing fractionated DOM samples.<sup>50</sup> The  
121 approach in the present study utilizes EfOM from differentially fouled bioreactor membranes and  
122 functionally fractionated bioreactor DOM to provide a novel assessment of inhibitory mechanisms of  
123 DOM in TiO<sub>2</sub> photocatalysis.

124 Bulk supernatant DOM and EfOM samples collected in 2015 and 2016 from an operational MBR in a  
125 municipal wastewater treatment plant (WWTP) are studied here. Fractionation of samples in terms of  
126 DOM size and hydrophobicity, a method commonly used to isolate organics, was applied to MBR  
127 bulk supernatant. Here, the effects of different fractions of bulk supernatant DOM and EfOM samples  
128 on photocatalytic processes are assessed to identify the most important fractions to reject during  
129 filtration. Three-dimensional fluorescence excitation-emission matrix (3DEEM) analysis is employed  
130 to characterize the resultant DOM from fractionation procedures and the MBR effluent samples, to  
131 better forecast and understand their effect on photocatalysis processes. 3DEEM is increasingly  
132 employed to understand DOM evolution in wastewater systems.<sup>51, 52</sup> A recent study also highlighted  
133 that 3DEEM can be used to distinguish proteins from biopolymers and humic substances and to  
134 quantify building blocks, with potential use as an on-line indicator to describe DOM fate and  
135 behavior.<sup>53</sup> Further, this technique has distinguished the effects of different types of DOM on water  
136 treatment technologies (i.e., membrane fouling, UV attenuation, and disinfection byproduct

137 formation).<sup>43, 54-56</sup> Inhibitory profiles of the DOM fractions and EfOM samples are established by  
138 measuring the photodegradation of a molecular probe as a function of total organic carbon (TOC)  
139 concentration. Inhibition mechanisms are discussed in the context of an experimentally validated  
140 model that accounts for surface and bulk phase quenching processes simultaneously.<sup>29</sup> Finally,  
141 comments are made on the prospective utility of photocatalytic membrane reactors (PMRs)<sup>57-59</sup> as a  
142 combined treatment process.

143

## 144 **2. Materials and methods**

145

### 146 2.1. Chemicals

147 Humic acid and 4-chlorobenzoic acid were obtained from Alfa Aesar (Haverhill, MA). Titanium  
148 dioxide (99.9% Anatase) was purchased from Alfa Aesar with a nominal particle size of 32 nm and  
149 surface area of 45 m<sup>2</sup>/g. Ultrapure water (>18.2 MΩ-cm) was produced using a Nanopure Infinity  
150 system (Thermo Fisher Scientific Inc., Waltham, MA). HPLC solvents were HPLC-grade and  
151 obtained from Alfa Aesar.

### 152 2.2. EfOM sampling

153 EfOM samples were collected from a full-scale MBR wastewater treatment plant (La Grande Motte,  
154 France), which treats municipal wastewater and serves a population of approximately 60,000. The  
155 plant performs biological removal of nitrogen (nitrification and denitrification) and phosphorus. The  
156 plant comprises four MBR tanks, each equipped with KUBOTA Submerged Membrane Units®  
157 (SMUs, KUBOTA, Japan), which are flat sheet microporous membranes made of chlorinated  
158 polyethylene with an average pore size of 0.2 μm and a nominal pore size of 0.4 μm. Only two MBR  
159 tanks were studied. Here we define MBR1 as the unit which underwent chemical cleaning and MBR2  
160 as a reference unit that did not undergo chemical cleaning during the sampling period. MBR2 was two  
161 months into a three- to four-month cycle and therefore was chosen to represent a membrane during  
162 normal operation. To assess the cleaning effect, activated sludge (AS) and permeate samples were  
163 taken from MBR1 and MBR2 one day before and one day after the cleaning procedure took place for

164 MBR1 (June 2016). After sampling, AS samples were filtered with a 1.2  $\mu\text{m}$  glass microfiber filters  
165 (Whatman GF/C) to collect the dissolved portion of the AS, labeled as the bulk supernatant (BSN).  
166 Hence, four samples from the MBR1 cleaning campaign and two samples from MBR2 were collected  
167 and analyzed for this study: and each sample was given a reference name as shown in Table 1.

168 In addition to the samples taken to assess the effects of membrane cleaning, 500 L of AS were also  
169 collected from MBR1 in June 2015 to perform DOM fractionation using dialysis and XAD-resins.  
170 Prior to fractionation the AS was filtered successively through 50  $\mu\text{m}$  and 2  $\mu\text{m}$  polypropylene filters  
171 to collect BSN. Next, softening was performed using a sodium cation-exchange resin (Purolite,  
172 France) to remove calcium and magnesium ions, to avoid ion complexation with DOM and scaling  
173 during the following step: reverse osmosis (RO).<sup>60</sup> DOM in the BSN sample was concentrated via RO  
174 in order to minimize the time required for the fractionation step. A Filmtec TW 30 membrane was  
175 used for the RO process, since it is known to be more resistant to DOM adsorption.<sup>61</sup> The RO process  
176 effectively concentrated the BSN by 100-fold which was subsequently used to perform DOM  
177 fractionation.

### 178 2.3. DOM fractionation

179 The first fractionation step consisted of isolating the colloidal portion of DOM by size exclusion, using  
180 dialysis (3.5 kDa, Spectra/Por 6 Dialysis Membrane) against HCl (0.01 mol/L, pH 2). Next, organic  
181 colloids were separated from colloidal silica and precipitated salts by dialysis (3.5 kDa) against 0.2  
182 mol/L HF.<sup>62</sup> The dialysate, approximately 30 L of HCl solution containing DOM compounds with a  
183 molecular weight smaller than 3.5 kDa, was then passed through XAD8 and XAD4 resins (Amberlite,  
184 Sigma Aldrich) arranged in tandem. This step allowed for the collection of hydrophobic (HPO) and  
185 transphilic (TPI) fractions.<sup>42, 63</sup> The hydrophilic (HPI) fraction, composed of low molecular weight  
186 hydrophilic DOM and salts, was collected in the outlet of the resins tandem. This fraction, however,  
187 was not used in the study because the solution contained highly concentrated salts, which co-  
188 precipitate with the organic matter. Removing these salts, while possible, would have required a  
189 complex purification step called azeotropic distillation.<sup>64</sup> To collect HPO and TPI fractions adsorbed

190 onto XAD resins, elution with an acetonitrile/MQ water solution (75/25% v/v) was performed,  
191 followed by evaporation and freeze-drying of the respective organic matter samples.

192

193 Table 1. Nomenclature of samples and fractions based on their respective MBR units, sampling  
194 period, or fractionation procedure.

Label	Collection	Description
BSNf-MBR1	MBR1, Bulk Supernatant	Fouled membrane (Pre-wash)
BSNw-MBR1	MBR1, Bulk Supernatant	Washed membrane (Post-wash)
BSN-MBR2	MBR2, Bulk Supernatant	Midpoint between chemical cleaning events
Pf-MBR1	MBR1, Permeate	Fouled membrane (Pre-wash)
Pw-MBR1	MBR1, Permeate	Washed membrane (Post-wash)
P-MBR2	MBR2, Permeate	Midpoint between chemical cleaning events
C	MBR1, Bulk Supernatant	Colloidal fraction
HPO	MBR1, Bulk Supernatant	Hydrophobic fraction
TPI	MBR1, Bulk Supernatant	Transphilic fraction

195

## 196 2.4. DOM characterization

### 197 2.4.1 TOC and UV<sub>254</sub> absorbance measurements

198 TOC analysis was performed using a TOC-VCSH Shimadzu analyzer (Shimadzu Japan). The UV<sub>254</sub>  
199 absorbance was measured in a 1 cm quartz cuvette using a UV-VIS spectrophotometer (UV-2401PC,  
200 Shimadzu, Japan). The specific UV absorbance (SUVA<sub>254</sub>) was then calculated as the ratio of UV<sub>254</sub>  
201 absorbance and TOC value.<sup>65</sup> These analyses are reported in Table S1.

### 202 2.4.2. 3DEEM analysis

203 Fluorescence spectra were obtained using a Perkin-Elmer LS-55 spectrometer (USA) and a procedure  
204 described elsewhere.<sup>53</sup> Spectra were divided into five regions as defined by Chen et al.,<sup>54</sup>  
205 corresponding to different groups of fluorophores. The regions were categorized by excitation-  
206 emission ranges, as noted in Table 2. Region I is associated with aromatic protein-like fluorophores  
207 type I (tyrosine type); Region II is associated to aromatic protein-like fluorophores type II (tyrosine  
208 type); Region III corresponds to fulvic acid-like fluorophores; and Region IV and V are associated  
209 with SMP-like fluorophores (tryptophane type) and humic acid-like fluorophores, respectively.

210 Table 2. Excitation and emission wavelength classifications of fluorophores.

	<b>Region I</b>	<b>Region II</b>	<b>Region III</b>	<b>Region IV</b>	<b>Region V</b>
Excitation, nm	200 – 250			250 – 350	250 – 500
Emission, nm	280 – 330	300 – 350	380 – 600	280 – 380	380 – 600

211

212 For qualitative analysis, spectra are represented in A.U. (Arbitrary Unit) and rejected fraction spectra  
 213 (R) were calculated by subtracting permeate spectra from the BSN spectra, in order to better visualize  
 214 the constituents that are rejected by the membrane. For semi-quantitative analysis, the volume of  
 215 fluorescence  $\Phi(i)$  (Raman Unit.nm<sup>2</sup>) normalized by the Raman spectra,<sup>66</sup> consisting of the integration  
 216 of the spectral regions, was calculated in the different spectral regions using the following equation  
 217 taken from the fluorescence regional integration (FRI)<sup>54</sup> method:

$$\Phi(i) = MF(i) \sum_{ex} \sum_{em} I(\lambda_{ex}\lambda_{em})\Delta\lambda_{ex}\Delta\lambda_{em}$$

218 (Eq. 1)

219 where MF(i) is a multiplication factor,  $\Delta\lambda_{ex}$  is the excitation wavelength interval (2 nm),  $\Delta\lambda_{em}$  is the  
 220 emission wavelength interval (0.5 nm) and  $I(\lambda_{ex}\lambda_{em})$  is the fluorescence intensity at each excitation-  
 221 emission pair (Raman units).  $\Phi(i)$  normalization was necessary to compare values from different  
 222 regions of the 3DEEM response. To do so, MF(i) was calculated using Equation 2.

$$MF(i) = \frac{Total\ spectra\ area}{Specific\ region\ area(i)}$$

223 (Eq. 2)

224 For percentage analysis, the ratio between the volume of fluorescence of each region and the total  
 225 volume was used.

## 226 2.5. Photochemical experiments

227 Photochemical experiments were conducted in an enclosed UV cabinet with a magnetically stirred  
 228 photoreactor at room temperature. A 15 W low pressure mercury lamp (Sankyo Denki Co.,) was used  
 229 as a UVC light source. The distance between the light source and reaction vessel was 20 cm. The  
 230 irradiance at 254 nm at the location of the vessel was measured to be 295  $\mu\text{W}/\text{cm}^2$  with a BLUE-Wave  
 231 UVNb-25 Spectrometer (StellarNet Inc., Tampa, FL). The UV/Vis emission spectrum for the lamp,  
 232 shown in Figure S1, was also recorded. The DOM fractions and EfOM samples described above,

233 along with HA, were used to show the inhibitory effect of organic matter on photocatalytic  
 234 degradation of target pollutants. Experiments utilized 15 ml of solution, containing 5  $\mu\text{g/L}$   $\text{TiO}_2$  with  
 235 10  $\mu\text{M}$  para-chlorobenzoic acid (*p*CBA) as a probe compound that has a known reaction rate constant  
 236 with  $\cdot\text{OH}$ .<sup>30</sup> HA, DOM fractions, or EfOM samples in various concentrations were added to the  
 237 reaction solutions to assess the quenching potential of each fraction. Sample aliquots of 0.5 mL were  
 238 taken at fixed time points and analyzed for *p*CBA concentration via HPLC, according to methods  
 239 reported elsewhere.<sup>67</sup> Briefly, this analysis was conducted with an Agilent HPLC (Agilent technology,  
 240 1260 infinity) using a C18 (125 mm) column using acetonitrile and 10 mM phosphoric acid as mobile  
 241 phase solvents (60:40). The flow rate was 0.5 mL/min and the detection wavelength was 234 nm. For  
 242 all photochemical reactions, *p*CBA degradation rates were obtained by linear regression of plots of  
 243 *p*CBA concentration versus radiant fluence ( $\mu\text{J}/\text{cm}^2$ ). Fluence values were calculated according to  
 244 Bolton and Linden (2003),<sup>68</sup> as described previously.<sup>57</sup> Importantly, these calculations account for  
 245 reductions in  $\text{UV}_{254}$  transmission by using sample-specific  $\text{UV}_{254}$  absorbance values and the  
 246 transmission distance inside the reactor. The resulting observed photodegradation rates ( $k_{\text{obs}}$ ) were, to a  
 247 good approximation, first order with respect to radiant exposure ( $H$ ,  $\mu\text{J}/\text{cm}^2$ ) such that the units of  $k_{\text{obs}}$   
 248 are reported as ( $\text{cm}^2/\mu\text{J}$ ), according to equations (3-6):

$$249 \quad \frac{dC}{dt} = k'_{\text{obs}}C, \quad (\text{Eq. 3})$$

$$250 \quad \frac{1}{H(\mu\text{J}/\text{cm}^2)} \frac{dC}{dt} = \frac{1}{H(\mu\text{J}/\text{cm}^2)} k'_{\text{obs}}C, \quad (\text{Eq. 4})$$

$$251 \quad \frac{dC}{dH} = k_{\text{obs}}C, \quad (\text{Eq. 5})$$

252 and

$$253 \quad k_{\text{obs}} \left( \frac{\text{cm}^2}{\mu\text{J}} \right) = \frac{k'_{\text{obs}} \left( \frac{1}{\text{s}} \right)}{E \left( \frac{\mu\text{W}}{\text{cm}^2} \right)}. \quad (\text{Eq. 6})$$

254 Here,  $k'_{\text{obs}}$  ( $\text{s}^{-1}$ ) is the first-order degradation rate constant of *p*CBA,  $C$  is the molar concentration of  
 255 *p*CBA, and  $E$  is the irradiance ( $\mu\text{W}/\text{cm}^2$ ) at 254 nm. The differences in the  $k_{\text{obs}}$  in the presence or  
 256 absence of organic compounds were used to quantify the inhibitory effect of these compounds.  
 257 Control experiments were also conducted in the absence of organic matter,  $\text{TiO}_2$ , or light.

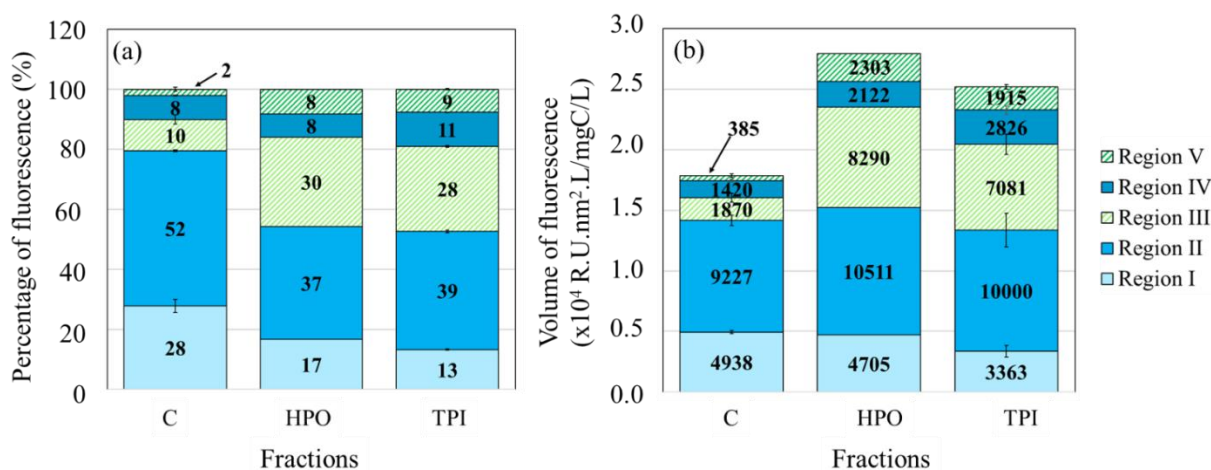
258

259 **3. Results**

260 3.1. Isolated DOM fractions

261 Prior to performing photocatalytic experiments, DOM fractions were characterized using 3DEEM to  
 262 identify molecular characteristics of DOM within each fraction. The 3DEEM spectra compiled for the  
 263 fractions are available elsewhere<sup>23</sup> and were used here to quantify the volume of fluorescence and the  
 264 percentage of fluorescence of each region in Figure 1.

265



266  
 267 Figure 1. (a) Percentage of fluorescence and (b) Volume of fluorescence of the colloidal (C), HPO and TPI  
 268 fractions prepared at 1 mgC/L. Region I, Region II, Region III, Region IV and Region V correspond to aromatic  
 269 proteins-like type I, aromatic proteins-like type II, fulvic-like, SMP-like and humic-like fluorophores,  
 270 respectively.

271  
 272 3DEEM analysis showed that each of the three DOM fractions contained both classes of fluorescent  
 273 compounds: proteins (Regions I, II and IV) and humic substances (Region III and V). However, as  
 274 seen in Figure 1a, DOM fractions exhibited different fluorescent properties, reflecting differences in  
 275 their compositions. The percentages of fluorescence of HPO and TPI fractions were similar for all  
 276 regions and had a dominant proportion of aromatic protein-like type II and fulvic-like fluorophores  
 277 (Figure 1a). That HPO and TPI compositions did not vary significantly in terms of fluorophore content  
 278 expected; a study on EfOM of wastewater treatment plants also found that these fractions were similar  
 279 in terms of fluorophore composition.<sup>69</sup> For the colloidal fraction, 80% of the fluorescent compounds  
 280 were aromatic protein-like type I and II fluorophores. Recent studies showed that both protein-like and  
 281 humic-like fluorophores impact photocatalytic performance. Protein-like constituents were found to

282 react with  $\cdot\text{OH}$  radicals in bulk solution,<sup>55</sup> with reported reaction rate constants of amino acids,  
283 proteins, and peptides with  $\cdot\text{OH}$  ranging from  $1.7 \times 10^7$  to  $1.05 \times 10^{10} \text{ M}^{-1} \text{ s}^{-1}$  (the rate constant between  
284 *p*CBA and  $\cdot\text{OH}$  is similar at  $5.2 \times 10^9 \text{ M}^{-1} \text{ s}^{-1}$ ),<sup>70-72</sup> while humic-like compounds, having a large number  
285 of carboxylic groups, adsorbed onto  $\text{TiO}_2$  surfaces, particularly at low pHs.<sup>73</sup> Thus, the high proportion  
286 of fluorescing compounds in Region I and II in colloids, suggests that the colloids may be more  
287 reactive with  $\cdot\text{OH}$  than HPO and TPI. On the contrary, HPO and TPI are expected to exhibit more  
288 surface-phase quenching by adsorbing more strongly onto  $\text{TiO}_2$  and than the colloids.

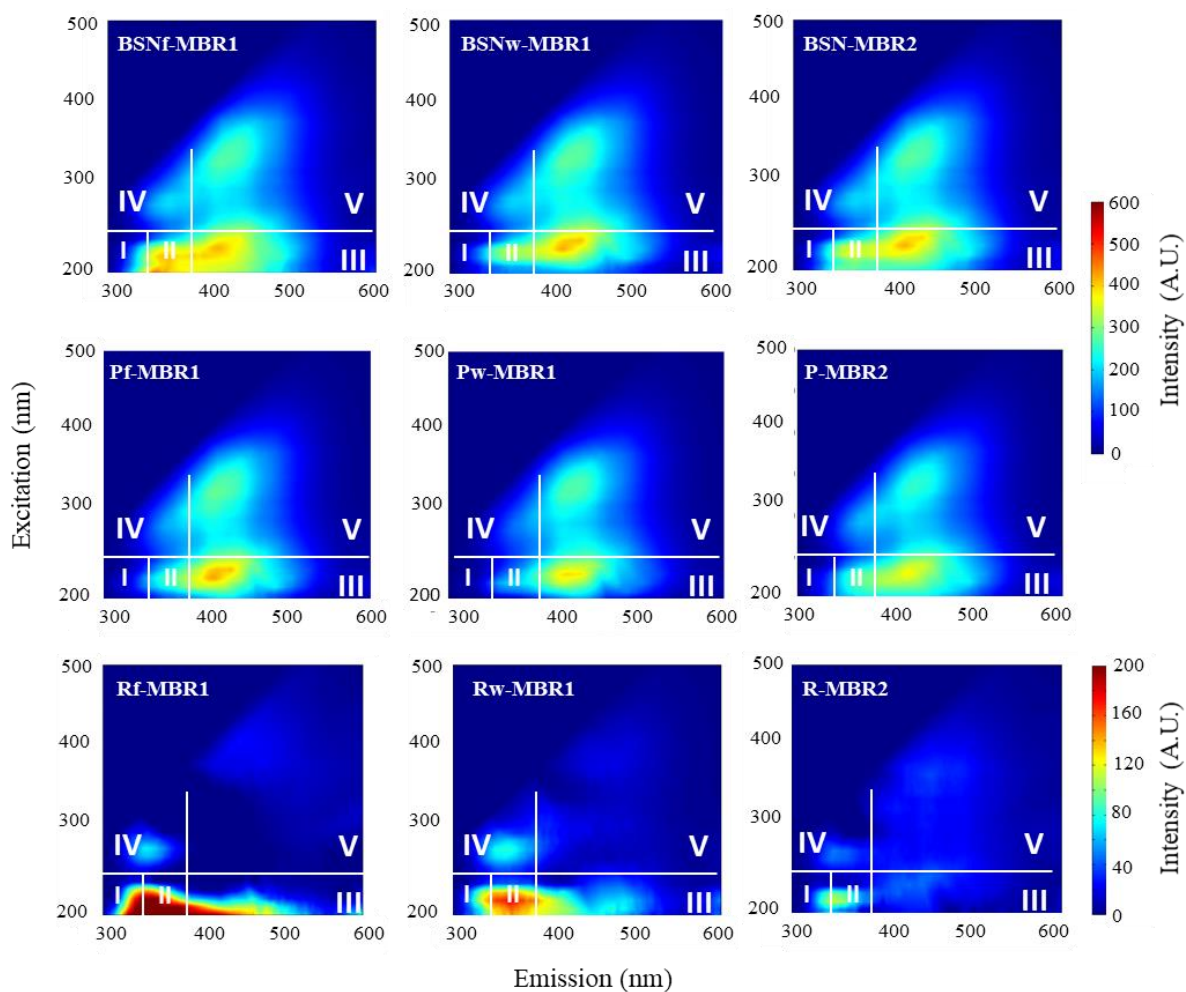
289 The volume of fluorescence is an indicator proportional to the concentration of fluorophores contained  
290 in each region. The higher electron density of fluorophores compared with other moieties could yield  
291 higher reactivity with ROS, and it would follow, then, that the higher the volume of fluorescence, the  
292 higher the quenching of photocatalysis. Thus, from Figure 2b, and hypothesizing that surface-phase  
293 quenching is the most problematic for photocatalysis, the DOM quenching potency could be expected  
294 in the following order: HPO>TPI>C. A similar analysis can be conducted by measuring the  $\text{SUVA}_{254}$   
295 values as a representation of average aromatic moiety content, which is known to loosely indicate  
296 DOM hydrophilicity.<sup>74</sup> In general, DOM compounds with higher  $\text{SUVA}_{254}$  values are considered to be  
297 more hydrophobic than those with lower values.<sup>75</sup> In addition, higher  $\text{SUVA}_{254}$  values correspond to  
298 more aromaticity, which could indicate higher reactivity with ROS, given the electron rich moieties.  
299 The  $\text{SUVA}_{254}$  values for the colloidal, HPO, and TPI fractions were measured to be 1.8, 2.2, and 1.6  
300  $\text{L}\cdot\text{mg}^{-1}\cdot\text{m}^{-1}$ , respectively. Based on this method of analysis, and assuming that electron-dense  
301 functional groups are the primary factor in determining ROS quenching, the inhibition capacity of the  
302 fractions could be expected in this order: HPO>C>TPI. Neither of these methods are expected to  
303 conclusively predict the true inhibition potential, given the many additional factors involved with  
304 quenching mechanisms.

### 305 3.2. EfOM composition and effect of membrane fouling

306 To estimate the effect of membrane fouling and cleaning on the retention of fluorophores, 3DEEM  
307 spectra of MBR bulk supernatant and permeate were compared (Figure 2). The membranes rejected  
308 most compounds from Regions I and II in the three MBR cases studied. This selectivity was apparent

309 in the 3DEEM spectra obtained by subtracting the permeate spectrum from the BSN spectrum. It is  
 310 likely that most of these aromatic-like fluorophores were associated with organic colloids since they  
 311 represented 80% of the overall colloidal content. This observation is consistent with a previous study  
 312 that demonstrated that colloids were major membrane foulants.<sup>23</sup>

313



314

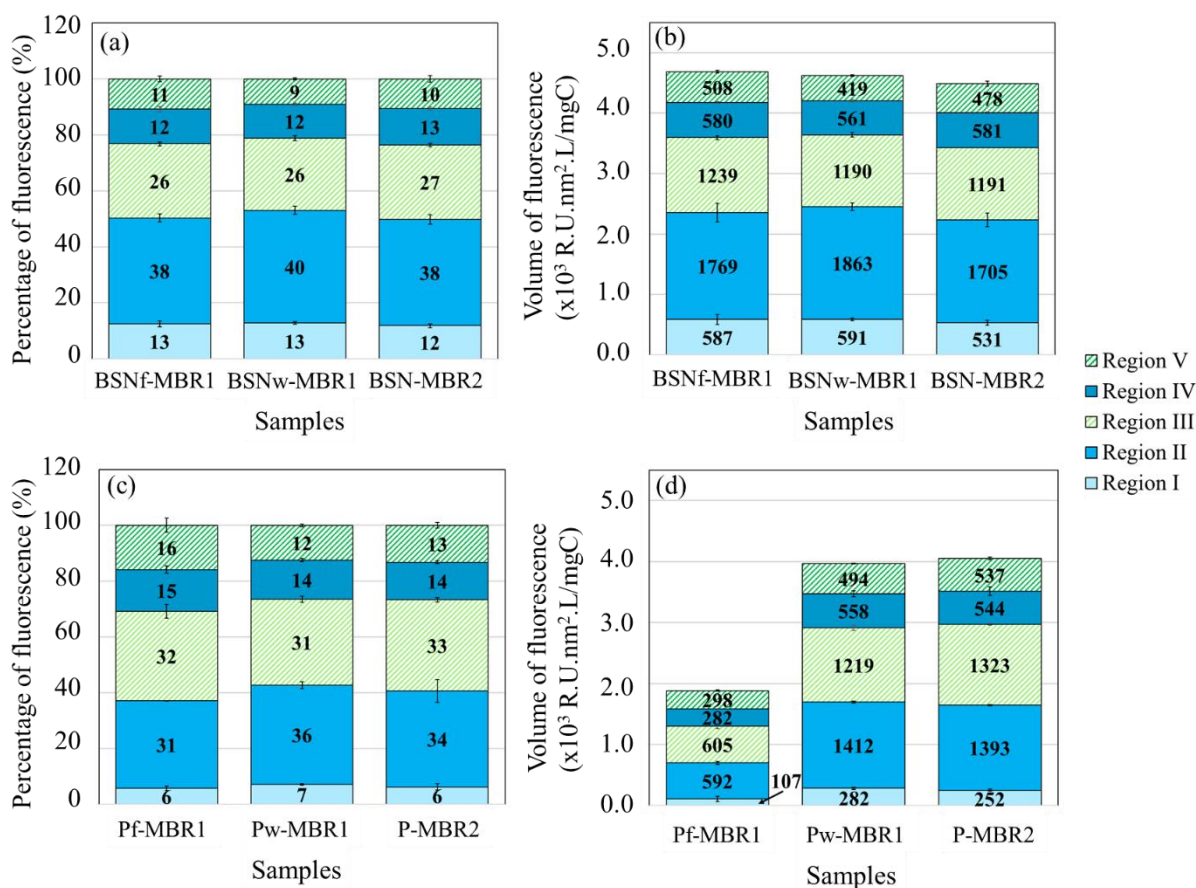
315 Figure 2. Fluorescence spectra of DOM from BSN and EfOM from permeate samples, with I, II, III, IV, V  
 316 corresponding to Region I (aromatic proteins-like type I), Region II (aromatic proteins-like type II), Region III  
 317 (fulvic-like), Region IV (SMP-like) and Region V (humic-like). R spectra correspond to the mathematical  
 318 subtraction of the permeate spectra from the bulk supernatant spectra allowing the identification of compounds  
 319 retained by the membrane. Note the different color scale for the R spectra.

320

321

322

323



324

325 Figure 3. Percentage (a, c) and volume (b, d) fluorescence values for bulk supernatant (a, b) and  
 326 permeate (c, d) samples.

327

328 Figures 3a and 3c show the fluorophore compositions in EfOM samples as percentages of the different  
 329 regions; these data showed a preferential rejection of the fluorophores from Region I and Region II.

330 Indeed, for the three samples, the membrane reduced the fluorescence by  $11 \pm 2$  % in both Region I  
 331 and II. This reduction corresponded to an increase of fluorescence percentage of the Regions III and V

332 in the permeate. The relative increase of the humic substance-related fluorophores confirmed that the

333 membrane preferentially retains colloids, since they are typically high molecular weight molecules

334 associated with protein-like fluorophores (Figure 1a).<sup>53</sup> Membrane fouling clearly affected the type of

335 fluorophores retained in the MBR (Figure 3b and Figure 3d). The three fouling stages present similar

336 bulk supernatant volumes of fluorescence (Figure 3b) and permeate percentage of fluorescence

337 profiles (Figure 3c), but different volumes of fluorescence in the permeate (Figure 3d). The TOC

338 normalized volume of fluorescence for Pf-MBR1 was reduced by 60% (Figure 3b and Figure 3d),

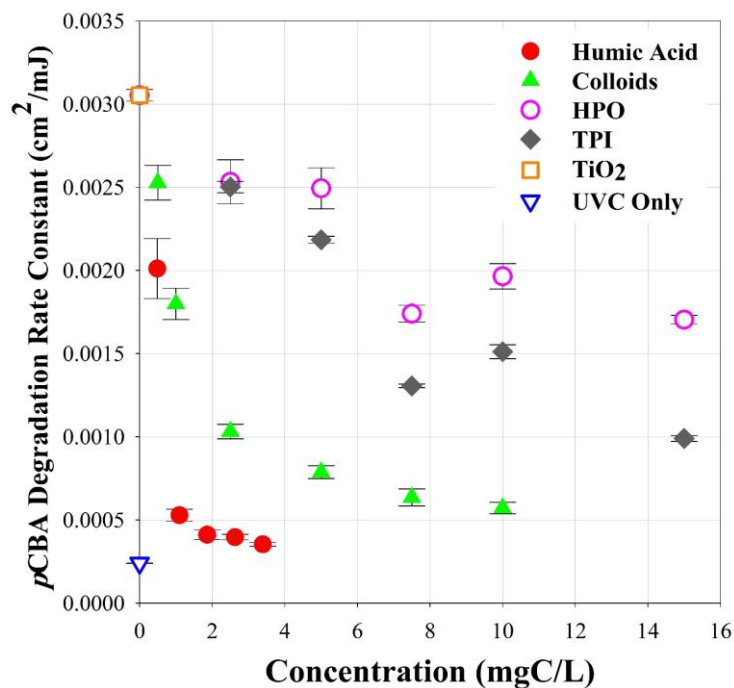
339 while the volume of fluorescence was only reduced by 14% and 10% for P-MBR2 and Pw-MBR1,  
340 respectively (Figure 3b and Figure 3d). Membrane fouling therefore has a clear effect on fluorophore  
341 quantity, via restricting EfOM permeation (Figure 3b). Indeed, more fluorescent compounds are  
342 retained, on a per carbon basis, by a fouled membrane. This result shows that the fouling layer on the  
343 membrane surface selectively removes compounds rich in functional groups with high electron  
344 density, which are more reactive with ROS than other moieties. Pw-MBR1 and P-MBR2 are therefore  
345 expected to quench photocatalysis to a greater extent. This assumption is supported by the  $SUVA_{254}$   
346 data: values for the Pf-MBR1, Pw-MBR1, and P-MBR2 samples were measured to be 0.8, 2.0, and 2.0  
347  $L \cdot mg^{-1} \cdot m^{-1}$ , respectively. Pf-MBR1, having a  $SUVA_{254}$  value of  $0.8 L \cdot mg^{-1} \cdot m^{-1}$ , is characterized by  
348 non-aromatic organic compounds and therefore fewer potential functional groups reactive with ROS.  
349 On the contrary, Pw-MBR1 and P-MBR2, with  $SUVA_{254}$  values of  $2.0 L \cdot mg^{-1} \cdot m^{-1}$ , contain more  
350 aromatic compounds, which may preferentially compete with ROS.

351 Control of membrane fouling may provide an opportunity to increase photocatalysis process efficiency  
352 by regulating the chemical makeup and concentration of EfOM. Less frequent cleaning events could  
353 be ideal, since the fouled membranes provided the highest DOM retention. From the fluorescence  
354 volumes, it is expected that  $TiO_2$  photocatalysis would be quenched to a greater extent by Pw-MBR1  
355 and P-MBR2, than by Pf-MBR1.

### 356 3.3. Inhibition of $\cdot OH$ by DOM Fractions

357 Segregation of MBR DOM into functional categories allowed for a unique examination of the  
358 inhibition potential of these functional classes of compounds. Colloidal, HPO, and TPI fractions were  
359 each examined for concentration-dependent inhibitory activity. Control tests confirmed the  
360 photocatalytic action of  $TiO_2$  and differentiated the role of ROS from the direct photolysis by  $UV_{254}$   
361 light (Figure S3). The action by  $UV_{254}$  alone represented the lower bound of  $k_{obs,pCBA}$ , where  $\cdot OH$   
362 radicals were completely quenched by DOM. Likewise, the case of  $TiO_2$  and  $pCBA$  in pure water  
363 served as the upper bound of photocatalytic efficiency, with no interfering quenching agents. The  
364  $k_{obs,pCBA}$  values plotted in Figure 4 showed that of the three DOM fractions, colloids exerted the  
365 strongest inhibition by far. The corresponding  $k'_{obs}$  ( $s^{-1}$ ) data is shown in Figure S4. The TPI and HPO

366 portions were similar in their effect on  $k_{\text{obs},p\text{CBA}}$ , and exerted mild inhibition at low TOC  
367 concentrations. Interestingly, for both TPI and HPO, the  $k_{\text{obs},p\text{CBA}}$  increased from 7.5 to 10 mgC/L. This  
368 increase in photodegradation efficacy was surprising but not unprecedented; it was recently reported  
369 that Natural Organic Matter (NOM) actually enhanced the  $\text{TiO}_2$ -driven photodegradation of  
370 carbamazepine, pharmaceutical compound, at specific  $\text{TiO}_2$ :NOM ratios, by up to 8%.<sup>76</sup> Favorable  
371 NOM-carbamazepine interactions explained the increased effectiveness; these interactions draw the  
372 compound closer to the active surface sites of  $\text{TiO}_2$ , where  $\cdot\text{OH}$  are present at higher concentrations.  
373 The colloidal fraction did not increase the photoactivity at any concentration. Examination of the  
374 inhibition profiles of the three DOM fractions in the context of 3DEEM analysis (Figure 1) suggested  
375 that the quenching action of the DOM fractions is correlated to higher concentration of colloids, which  
376 are characterized by a higher proportion of fluorescence in Region I and Region II (Figure 1a). This  
377 observation suggests that despite higher volumes of fluorescence, HPO and TPI are less potent  
378 inhibitors of photocatalysis than the colloids. The surface interactions, and therefore inhibition  
379 mechanism, of the colloids with the  $\text{TiO}_2$  surface could be fundamentally different from that of the  
380 HPO and TPI fractions, because the colloidal fraction was not segregated based on surface character,  
381 but rather by size only. Control of membrane surface properties and fouling could reduce the colloidal  
382 content—much of which consists of high molecular weight molecules that can be preferentially  
383 retained—in EfOM and thereby mitigate the quenching of photocatalytic processes by DOM.<sup>23</sup>



384

385 Figure 4: *p*CBA degradation rate constants in the presence of 5 mg/L TiO<sub>2</sub> and various concentrations  
 386 of colloids, TPI, HPO, and HA are depicted here. The rate constant for *p*CBA degradation by UVC  
 387 without TiO<sub>2</sub> is also shown. Ambient temperature was measured at 24 °C.

388

### 389 3.4. Inhibition of ·OH by EfOM

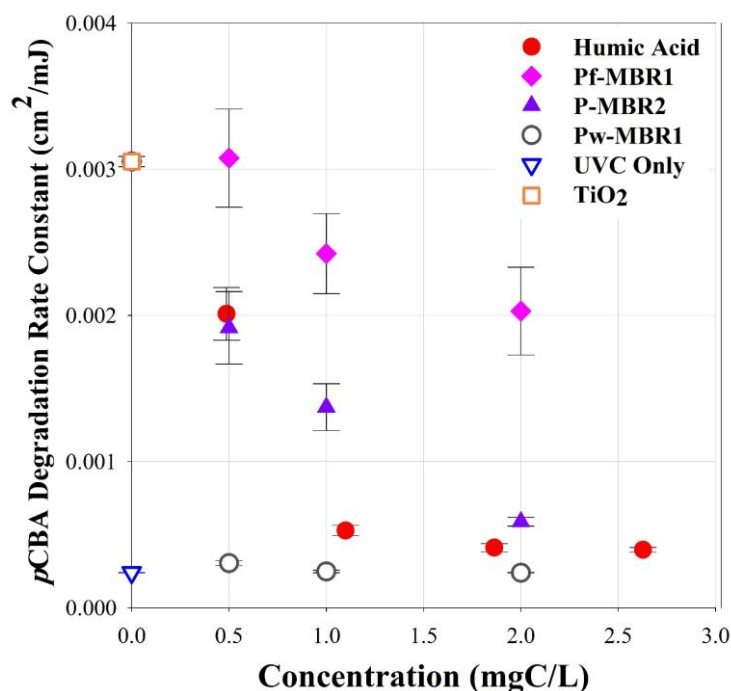
390 The EfOM of the three MBR permeate samples, as described above, was tested for inhibition potential  
 391 of ·OH-mediated *p*CBA degradation. The samples were examined on a TOC basis to discern changes  
 392 in inhibition potential caused by qualitative differences in EfOM composition. A low concentration of  
 393 TiO<sub>2</sub>, relative to that used in similar studies on photocatalyst-DOM interactions,<sup>29, 38, 77, 78</sup> was selected  
 394 to avoid the effects of EfOM transformation by oxidation. Hour-long UVC irradiation experiments  
 395 with 10 mg/L HA and various concentrations of TiO<sub>2</sub> showed that *p*CBA photodegradation kinetics  
 396 were linear for the TiO<sub>2</sub> concentration of 5 mg/L. Tests with TiO<sub>2</sub> concentrations of 100 mg/L or  
 397 higher showed accelerating kinetics and suggested that HA was itself being degraded by ·OH radicals  
 398 so that its inhibition potential changed with time.

399 The inhibition capacities of MBR EfOM samples were evaluated by measuring  $k_{obs,pCBA}$  as a function  
 400 of individual EfOM sample concentrations. These rates were calculated across concentrations ranging

401 from 0 to 2.3 mgC/L (Figure 5). The corresponding  $k'_{\text{obs}}$  (1) data is shown in Figure S5. Comparing  
402  $k_{\text{obs,pCBA}}$  values for the same TOC content reveals that the state of membrane fouling drove clear  
403 distinctions in inhibitory activity of the EfOM. While it was expected that a fouled membrane would  
404 reject more DOM than a clean membrane, the inhibition capacity on a per carbon basis was not  
405 known. Here, it was observed that EfOM from a fouled membrane system inhibited the photocatalytic  
406 process much less than EfOM from a cleaned membrane. At just 0.5 mgC/L, Pw-MBR1 quenched the  
407 photocatalytic process completely, while no quenching was observed by Pf-MBR1 EfOM at the same  
408 concentration. This result provides evidence that the changes in EfOM composition caused by  
409 membrane fouling; the reduction of colloid concentration and total fluorophores is especially  
410 beneficial for photocatalytic operation. 3DEEM confirmed that molecules containing fluorescent  
411 groups in Regions I and II impact photocatalytic performance more than other compounds. Qualitative  
412 changes in DOM retention by the membrane, therefore, impacted the photocatalytic quenching  
413 process. Considering these results in the context of the DOM fractions analysis, retention of organic  
414 colloids by the fouled membrane was likely enhanced by the formation of a fouling layer.<sup>3, 22</sup>  
415 Inhibition by P-MBR2, sourced from a membrane at the midpoint between chemical cleanings, was  
416 between the two extremes of Pw- and Pf-MBR1, with a ~75% reduction in  $k_{\text{obs,pCBA}}$  at 0.5 mgC/L.  
417 Alternatively, it may be possible to choose or modify membrane materials to selectively reject the  
418 organic colloidal materials regardless of the fouling state. HA served as a reference material, which  
419 represents NOM found in drinking water sources more closely than EfOM, and exhibited stronger  
420 quenching than the P-MBR2 case but less inhibition than Pw-MBR1. It is noteworthy that HA inhibits  
421 TiO<sub>2</sub> driven photocatalysis to a greater extent than EfOM from a fouled MBR on a carbon basis. This  
422 finding contradicts a 'common sense' assumption that could be made based solely on TOC values: that  
423 photocatalysis would be more applicable for drinking water applications than for WWTP effluent.

424 The 3DEEM analyses (Figure 3) of the MBR EfOM samples predicted that the fouled membrane  
425 would reduce the quantity of fluorescent compounds in the EfOM and therefore lead to less inhibition  
426 of photocatalysis. However, for cases of similar fluorescence volumes, as for Pw-MBR1 and P-MBR2  
427 in particular, the use of 3DEEM did not explain differences in inhibitory action. In these cases, other

428 factors, such as the hydrophobic/hydrophilic character of the EfOM, may have been altered by the  
 429 membrane fouling but not detected by 3DEEM or TOC analysis. It is well known that membrane  
 430 fouling affects rejection of DOM components<sup>41, 43, 79</sup> and that the mechanism of action is not simply  
 431 size exclusion alone: changes in the surface characteristics (i.e. charge and hydrophobicity), due to  
 432 fouling layer formation, are also important.<sup>3,22</sup>



433

434 Figure 5: pCBA degradation rate constants in the presence of various concentrations of HA, effluents  
 435 from Pf-MBR1, from Pw-MBR1, and from P-MBR2 with 5 mg/L TiO<sub>2</sub> are depicted here. The rate  
 436 constant for pCBA degradation by UVC without TiO<sub>2</sub> is also shown.

437

### 438 3.5. Inhibitory mechanisms for DOM samples

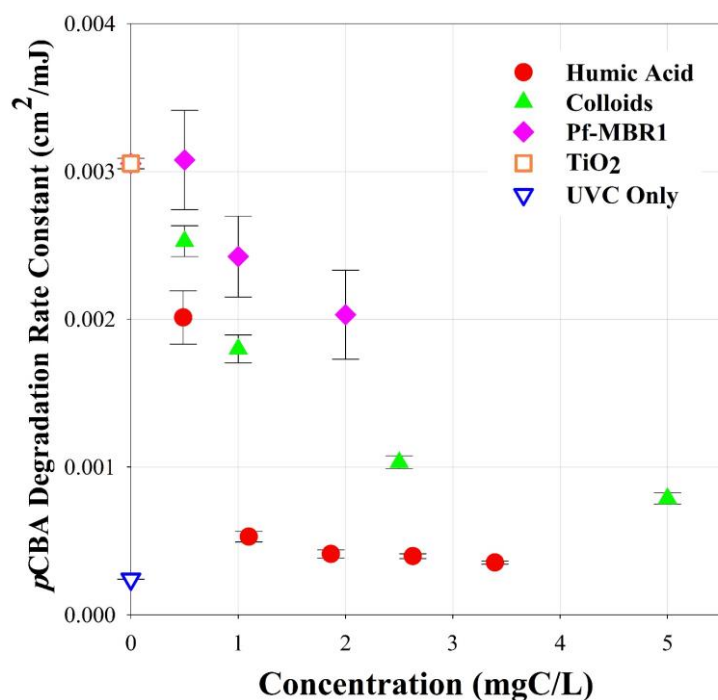
439 Identification of the mechanism of inhibition by DOM on TiO<sub>2</sub> photocatalysis is the key to designing  
 440 processes to overcome the problem of ROS quenching. Numerous studies have evaluated the  
 441 adsorption interactions of NOM onto TiO<sub>2</sub>, fitting experimental findings to Freundlich<sup>80</sup> or Langmuir-  
 442 Hinshelwood<sup>32, 77, 81</sup> isotherms. Only recently, however, was a model developed that accounted for  
 443 both bulk- and surface-phase quenching interactions.<sup>29</sup> In their work, Brame et al. experimentally  
 444 validated a model that combined a multi-solute Langmuir model<sup>82</sup> with bulk phase competitive

445 reaction rates by assuming steady-state ROS concentrations.<sup>29</sup> Based on this dual-phase model, the  
446 mode of inhibition (bulk or surface reactions) was successfully predicted by analysis of the  
447 dependency of  $k_{\text{obs}}$  on TOC. A linear dependence of  $k_{\text{obs}}$  on TOC implied that inhibition primarily  
448 occurred in the bulk phase and surface interactions were unimportant; alternatively, an exponential  
449 decay of  $k_{\text{obs}}$  with increasing TOC indicated that surface sorption and reactions played a significant  
450 role in the inhibitory process.<sup>29</sup> Note that the aforementioned report used Suwannee River humic acid  
451 as an NOM source, which consists of a wide range of molecules;<sup>29</sup> applying Brame's model in  
452 experiments with fractionated DOM samples is an important extension of the earlier work allowing for  
453 a discriminating analysis of inhibition mechanisms across the DOM spectrum. Here, all experiments  
454 were performed with the same probe compound, photocatalyst concentration, and UV<sub>254</sub> lamp, so  
455 normalization of  $k_{\text{obs},p\text{CBA}}$  was not necessary. The inhibition profile for HA was non-linear and  
456 therefore depended on surface interactions, in line with previous reports for TiO<sub>2</sub> inhibition by  
457 NOM.<sup>29, 38, 83, 84</sup> Upon examination of the inhibitory profiles of the MBR effluents, trends for Pf-MBR1  
458 and P-MBR2 were noted to be nearly linear, whereas Pw-MBR1 showed an exponential relationship.  
459 These observations suggest that the membrane fouling layer played a critical role by rejecting DOM  
460 that adsorbs favorably onto the surface of TiO<sub>2</sub>, thereby exerting a strong quenching effect on  
461 photocatalytic processes. These observations correlate well with the observed inhibition profiles of the  
462 fractionated DOM.

463 As discussed, the colloidal fraction of BSN DOM exerted the strongest inhibitory action of any of the  
464 fractions (Figure 4). The  $k_{\text{obs},p\text{CBA}}$  inhibition profiles of the DOM fractions reveal that the colloids  
465 quenched the photocatalytic process via sorption onto the TiO<sub>2</sub> surface and reacting with surface-  
466 bound ·OH. The HPO and TPI fractions, however, displayed a linear dependence—if the spurious  
467 enhancement of  $k_{\text{obs},p\text{CBA}}$  at the 10 mgC/L mark is neglected—on TOC. The HPO and TPI samples,  
468 therefore, primarily reduced  $k_{\text{obs},p\text{CBA}}$  through bulk phase reactions limited by diffusion and relative  
469 reaction rates. Note that these remarks on quenching mechanisms are generalizations: even the  
470 fractionated DOM samples contain a wide variety of molecules, each with specific adsorption  
471 affinities and reaction rates. Still, results of both fractionation and membrane fouling conditions

472 showed significant changes to inhibitory action of DOM. The inhibitory action of the colloidal fraction  
 473 was particularly interesting, given the lack of inhibitory action by effluent from the fouled membrane.  
 474 These observations taken together in Figure 6 (data replotted from Figures 4 and 5) suggest that fouled  
 475 membranes reject key organic colloids that would otherwise adsorb strongly to TiO<sub>2</sub> surfaces and  
 476 greatly reduce photodegradation rates. The corresponding  $k'_{\text{obs}}$  (s<sup>-1</sup>) data is shown in Figure S6. The  
 477 prospective utility of a membrane for pretreatment is clearly demonstrated by these results: if a  
 478 membrane can be selected or optimized to reject problematic colloids, photocatalysis may indeed be  
 479 effective for disinfection of MBR effluent.

480



481

482 Figure 6:  $k_{\text{obs},p\text{CBA}}$  inhibition profiles of HA, Pf-MBR1, and the colloidal fraction. Data from Figures 3  
 483 and 4 are used here.

484

#### 485 4. Conclusions

486 The challenge of unwanted ROS-DOM reactions has long plagued photocatalysis, particularly for  
 487 applications dealing with high TOC concentrations such as in a typical MBR effluent. 3DEEM can be

488 used to predict the inhibitory effects of DOM composition, and the experiments shed new light on the  
489 quenching of photocatalysts by DOM. First, the total fluorescence volume correlated well with the  
490 extent of photocatalytic inhibition on a carbon basis, further the DOM fractionation demonstrated that  
491 the colloidal fraction of DOM exerted stronger quenching action than HPO and TPI. The membrane  
492 fouling status showed that fouled membrane showed very little inhibitory action compared to permeate  
493 from clean and moderately fouled membranes. In fact, DOM from fouled membrane appeared to  
494 quench  $\cdot\text{OH}$  primarily via bulk-phase scavenging, whereas DOM from a clean membrane showed an  
495 inhibition profile consistent with surface-phase reactions,<sup>28</sup> suggesting that the membrane fouling layer  
496 rejected materials that would otherwise adsorb strongly to the  $\text{TiO}_2$  surface. To enhance  
497 photocatalysis efficiency, it might be possible to select a membrane with a “built-in” selectivity  
498 similar to that of the fouled membrane in order to remove the problematic colloidal fraction. Analysis  
499 of the inhibition profiles of the EfOM described here suggests that for the operation of a PMR a trade-  
500 off can be made between the operational pressure and the photocatalytic efficiency; by reducing the  
501 (chemical) cleaning frequency and thereby maintaining a minimal level of fouling, inhibition of  
502 photocatalysis by organic colloidal inhibitors would be mitigated at a cost of higher trans-membrane  
503 pressures. Further, the surface coverage of  $\text{TiO}_2$  on PMRs can be tuned to optimize photocatalyst  
504 surface area<sup>85</sup> and may not be limited to the DOM: $\text{TiO}_2$  ratios explored here.

505 Further research on the fundamental surface interactions between these organic colloidal materials and  
506 photocatalyst or membrane surfaces should be pursued in order to develop mitigation strategies for  
507 DOM-related ROS inhibition. Specifically, the assessment of the potential effects of the hydrophilic  
508 fraction and dissolved ions (i.e., multivalent cations and halides), which were not retained by the  
509 fractionation processes, should be examined. The results of the present study may be applicable to the  
510 use of photocatalytic materials in systems containing other DOM sources, therefore additional  
511 investigations on systems such as potable water supplies or industrial waste streams would be timely  
512 and important.

513

## 514 **5. Acknowledgements**

515 This material is based upon work supported in part by the Louisiana Board of Regents Research  
516 Competitiveness Subprogram under grant LEQSF(2017-20)-RD-A-06 and in part by the National  
517 Science Foundation Partnerships for International Research and Education program under Grant IIA-  
518 1243433. The authors would like to thank the operators at the La Grande Motte wastewater treatment  
519 plant for providing access to their facility and assistance with collecting wastewater samples for  
520 analysis.

521

## 522 6. References

- 523 1. R. L. Droste, *Theory and Practice of Water and Wastewater Treatment*, John Wiley & Sons,  
524 Inc., New York, 1997.
- 525 2. L. B. Franklin, *Wastewater Engineering: Treatment, Disposal and Reuse*, McGraw Hill, Inc.,  
526 New York, 1991.
- 527 3. O. T. Iorhemen, R. A. Hamza and J. H. Tay, Membrane Bioreactor (MBR) Technology for  
528 Wastewater Treatment and Reclamation: Membrane Fouling, *Membranes*, 2016, **6**, 1-29.
- 529 4. D. S. Francy, E. A. Stelzer, R. N. Bushon, A. M. G. Brady, A. G. Williston, K. R. Riddell, M.  
530 A. Borchardt, S. K. Spencer and T. M. Gellner, Comparative effectiveness of membrane  
531 bioreactors, conventional secondary treatment, and chlorine and UV disinfection to remove  
532 microorganisms from municipal wastewaters, *Water Res.*, 2012, **46**, 4164-4178.
- 533 5. E. O'Brien, M. Munir, T. Marsh, M. Heran, G. Lesage, V. V. Tarabara and I. Xagorarakis,  
534 Diversity of DNA viruses in effluents of membrane bioreactors in Traverse City, MI (USA)  
535 and La Grande Motte (France), *Water Res.*, 2017, **111**, 338-345.
- 536 6. Y. P. Zhang and J. L. Zhou, Occurrence and removal of endocrine disrupting chemicals in  
537 wastewater, *Chemosphere*, 2008, **73**, 848-853.
- 538 7. Y. L. Luo, W. S. Guo, H. H. Ngo, L. D. Nghiem, F. I. Hai, J. Zhang, S. Liang and X. C. C.  
539 Wang, A review on the occurrence of micropollutants in the aquatic environment and their  
540 fate and removal during wastewater treatment, *Sci. Total Environ.*, 2014, **473**, 619-641.
- 541 8. M. Munir, K. Wong and I. Xagorarakis, Release of antibiotic resistant bacteria and genes in the  
542 effluent and biosolids of five wastewater utilities in Michigan, *Water Res.*, 2011, **45**, 681-693.
- 543 9. I. Kim, N. Yamashita and H. Tanaka, Performance of UV and UV/H<sub>2</sub>O<sub>2</sub> processes for the  
544 removal of pharmaceuticals detected in secondary effluent of a sewage treatment plant in  
545 Japan, *J. Hazard. Mater.*, 2009, **166**, 1134-1140.
- 546 10. M. Klavarioti, D. Mantzavinos and D. Kassinos, Removal of residual pharmaceuticals from  
547 aqueous systems by advanced oxidation processes, *Environ. Int.*, 2009, **35**, 402-417.
- 548 11. L. Yang, L. E. Yu and M. B. Ray, Degradation of paracetamol in aqueous solutions by TiO<sub>2</sub>  
549 photocatalysis, *Water Res.*, 2008, **42**, 3480-3488.
- 550 12. Y. J. Meng, Y. Wang, Q. Han, N. Xue, Y. Y. Sun, B. Y. Gao and Q. L. Li, Trihalomethane  
551 (THM) formation from synergic disinfection of biologically treated municipal wastewater:  
552 Effect of ultraviolet (UV) irradiation and titanium dioxide photocatalysis on dissolve organic  
553 matter fractions, *Chem. Eng. J.*, 2016, **303**, 252-260.
- 554 13. J. C. Crittenden, R. Rhodes Trussell and D. W. Hand, *MWH's Water Treatment: Principles  
555 and Design*, John Wiley & Sons, Inc. , Hoboken, New Jersey, 2012.
- 556 14. W. A. M. Hijnen, E. F. Beerendonk and G. J. Medema, Inactivation credit of UV radiation for  
557 viruses, bacteria and protozoan (oo)cysts in water: A review, *Water Res.*, 2006, **40**, 3-22.

- 558 15. M. Cho, H. M. Chung, W. Y. Choi and J. Y. Yoon, Different inactivation Behaviors of MS-2  
559 phage and Escherichia coli in TiO<sub>2</sub> photocatalytic disinfection, *Appl. Environ. Microbiol.*,  
560 2005, **71**, 270-275.
- 561 16. S. D. Snow, K. Park and J.-H. Kim, Cationic Fullerene Aggregates with Unprecedented Virus  
562 Photoinactivation Efficiencies in Water, *Environ. Sci. Tech. Let.*, 2014, **1**, 290-294.
- 563 17. S. Malato, P. Fernandez-Ibanez, M. I. Maldonado, J. Blanco and W. Gernjak,  
564 Decontamination and disinfection of water by solar photocatalysis: Recent overview and  
565 trends, *Catal. Today*, 2009, **147**, 1-59.
- 566 18. M. Cho, H. Chung, W. Choi and J. Yoon, Linear correlation between inactivation of E. coli  
567 and OH radical concentration in TiO<sub>2</sub> photocatalytic disinfection, *Water Res*, 2004, **38**, 1069-  
568 1077.
- 569 19. J. A. Grant and R. Hofmann, A comparative study of the hydroxyl radical scavenging capacity  
570 of activated sludge and membrane bioreactor wastewater effluents, *Water Sci. Technol.*, 2016,  
571 **73**, 2067-2073.
- 572 20. S. Tang, Z. Wang, Z. Wu and Q. Zhou, Role of dissolved organic matters (DOM) in  
573 membrane fouling of membrane bioreactors for municipal wastewater treatment, *J. Hazard.*  
574 *Mater.*, 2010, **178**, 377-384.
- 575 21. K. Chon, K. Lee, I.-S. Kim and A. Jang, Performance assessment of a submerged membrane  
576 bioreactor using a novel microbial consortium, *Bioresour. Technol.*, 2016, **210**, 2-10.
- 577 22. C. Jarusutthirak, G. Amy and J.-P. Croué, Fouling characteristics of wastewater effluent  
578 organic matter (EfOM) isolates on NF and UF membranes, *Desalination*, 2002, **145**, 247-255.
- 579 23. C. Jacquin, B. Teychene, L. Lemee, G. Lesage and M. Heran, Characteristics and fouling  
580 behaviors of Dissolved Organic Matter fractions in a full-scale submerged membrane  
581 bioreactor for municipal wastewater treatment, *Biochem. Eng. J.*, 2018, **132**, 169-181.
- 582 24. P. Wang, Z. W. Wang, Z. C. Wu and S. H. Mai, Fouling behaviours of two membranes in a  
583 submerged membrane bioreactor for municipal wastewater treatment, *J. Membr. Sci.*, 2011,  
584 **382**, 60-69.
- 585 25. C. Kunacheva, C. Le, Y. N. A. Soh and D. C. Stuckey, Chemical Characterization of Low  
586 Molecular Weight Soluble Microbial Products in an Anaerobic Membrane Bioreactor,  
587 *Environ. Sci. Technol.*, 2017, **51**, 2254-2261.
- 588 26. J. Y. Sun, K. Xiao, Y. H. Mo, P. Liang, Y. X. Shen, N. W. Zhu and X. Huang, Seasonal  
589 characteristics of supernatant organics and its effect on membrane fouling in a full-scale  
590 membrane bioreactor, *J. Membr. Sci.*, 2014, **453**, 168-174.
- 591 27. K. Xiao, Y. X. Shen, S. Liang, P. Liang, X. M. Wang and X. Huang, A systematic analysis of  
592 fouling evolution and irreversibility behaviors of MBR supernatant hydrophilic/hydrophobic  
593 fractions during microfiltration, *J. Membr. Sci.*, 2014, **467**, 206-216.
- 594 28. S. Giannakis, S. Liu, A. Carratalà, S. Rtimi, M. Talebi Amiri, M. Bensimon and C. Pulgarin,  
595 Iron oxide-mediated semiconductor photocatalysis vs. heterogeneous photo-Fenton treatment  
596 of viruses in wastewater. Impact of the oxide particle size, *J. Hazard. Mater.*, 2017, **339**, 223-  
597 231.
- 598 29. J. Brame, M. Long, Q. Li and P. Alvarez, Inhibitory effect of natural organic matter or other  
599 background constituents on photocatalytic advanced oxidation processes: Mechanistic model  
600 development and validation, *Water Res*, 2015, **84**, 362-371.
- 601 30. G. V. Buxton, C. L. Greenstock, W. P. Helman and A. B. Ross, Critical review of rate  
602 constants for reactions of hydrated electrons, hydrogen atoms and hydroxyl radicals (.OH/.O-)  
603 in aqueous solution, *J. Phys. Chem. Ref. Data*, 1988, **17**, 513-886.
- 604 31. S. Kim and W. Choi, Kinetics and mechanisms of photocatalytic degradation of  
605 (CH<sub>3</sub>)<sub>n</sub>NH<sub>4</sub><sup>n+</sup> (0 ≤ n ≤ 4) in TiO<sub>2</sub> suspension: The role of OH radicals, *Environ. Sci.*  
606 *Technol.*, 2002, **36**, 2019-2025.
- 607 32. R. Enriquez and P. Pichat, Interactions of Humic Acid, Quinoline, and TiO<sub>2</sub> in Water in  
608 Relation to Quinoline Photocatalytic Removal, *Langmuir*, 2001, **17**, 6132-6137.
- 609 33. C. Kunacheva, Y. N. A. Soh, A. P. Trzcinski and D. C. Stuckey, Soluble microbial products  
610 (SMPs) in the effluent from a submerged anaerobic membrane bioreactor (SAMBR) under  
611 different HRTs and transient loading conditions, *Chem. Eng. J.*, 2017, **311**, 72-81.

- 612 34. Y. Yang, J. J. Pignatello, J. Ma and W. A. Mitch, Effect of matrix components on UV/H<sub>2</sub>O<sub>2</sub>  
613 and UV/S<sub>2</sub>O<sub>8</sub><sup>2-</sup> advanced oxidation processes for trace organic degradation in reverse  
614 osmosis brines from municipal wastewater reuse facilities, *Water Res.*, 2016, **89**, 192-200.
- 615 35. F. L. Rosario-Ortiz, E. C. Wert and S. A. Snyder, Evaluation of UV/H<sub>2</sub>O<sub>2</sub> treatment for the  
616 oxidation of pharmaceuticals in wastewater, *Water Res.*, 2010, **44**, 1440-1448.
- 617 36. N. Senesi, Binding mechanisms of pesticides to soil humic substances, *Sci. Total Environ.*,  
618 1992, **123-124**, 63-76.
- 619 37. J. D. Ritchie and E. M. Perdue, Proton-binding study of standard and reference fulvic acids,  
620 humic acids, and natural organic matter, *Geochim. Cosmochim. Acta*, 2003, **67**, 85-96.
- 621 38. J. Brame, M. C. Long, Q. L. Li and P. Alvarez, Trading oxidation power for efficiency:  
622 Differential inhibition of photo-generated hydroxyl radicals versus singlet oxygen, *Water Res.*,  
623 2014, **60**, 259-266.
- 624 39. P. R. Ogilby, Singlet oxygen: there is indeed something new under the sun, *Chem. Soc. Rev.*,  
625 2010, **39**, 3181-3209.
- 626 40. Z. X. Cai and M. M. Benjamin, NOM Fractionation and Fouling of Low-Pressure Membranes  
627 in Microgranular Adsorptive Filtration, *Environ. Sci. Technol.*, 2011, **45**, 8935-8940.
- 628 41. L. Fan, J. L. Harris, F. A. Roddick and N. A. Booker, Influence of the characteristics of  
629 natural organic matter on the fouling of microfiltration membranes, *Water Res.*, 2001, **35**,  
630 4455-4463.
- 631 42. E. Filloux, H. Gallard and J.-P. Croue, Identification of effluent organic matter fractions  
632 responsible for low-pressure membrane fouling, *Water Res.*, 2012, **46**, 5531-5540.
- 633 43. R. K. Henderson, N. Subhi, A. Antony, S. J. Khan, K. R. Murphy, G. L. Leslie, V. Chen, R.  
634 M. Stuetz and P. Le-Clech, Evaluation of effluent organic matter fouling in ultrafiltration  
635 treatment using advanced organic characterisation techniques, *J. Membr. Sci.*, 2011, **382**, 50-  
636 59.
- 637 44. H. K. Shon, S. Vigneswaran, I. S. Kim, J. Cho and H. H. Ngo, Fouling of ultrafiltration  
638 membrane by effluent organic matter: A detailed characterization using different organic  
639 fractions in wastewater, *J. Membr. Sci.*, 2006, **278**, 232-238.
- 640 45. P. Le-Clech, V. Chen and T. A. G. Fane, Fouling in membrane bioreactors used in wastewater  
641 treatment, *J. Membr. Sci.*, 2006, **284**, 17-53.
- 642 46. F. L. Wang and V. V. Tarabara, Pore blocking mechanisms during early stages of membrane  
643 fouling by colloids, *J. Colloid Interface Sci.*, 2008, **328**, 464-469.
- 644 47. Q. L. Li and M. Elimelech, Organic fouling and chemical cleaning of nanofiltration  
645 membranes: Measurements and mechanisms, *Environ. Sci. Technol.*, 2004, **38**, 4683-4693.
- 646 48. M. Aslam, A. Charfi, G. Lesage, M. Heran and J. Kim, Membrane bioreactors for wastewater  
647 treatment: A review of mechanical cleaning by scouring agents to control membrane fouling,  
648 *Chem. Eng. J.*, 2017, **307**, 897-913.
- 649 49. C. S. Uyguner-Demirel, N. C. Birben and M. Bekbolet, Elucidation of background organic  
650 matter matrix effect on photocatalytic treatment of contaminants using TiO<sub>2</sub>: A review, *Catal.*  
651 *Today*, 2017, **284**, 202-214.
- 652 50. P. Mwaanga, E. R. Carraway and M. A. Schlautman, Preferential sorption of some natural  
653 organic matter fractions to titanium dioxide nanoparticles: influence of pH and ionic strength,  
654 *Environ. Monit. Assess.*, 2014, **186**, 8833-8844.
- 655 51. E. M. Carstea, J. Bridgeman, A. Baker and D. M. Reynolds, Fluorescence spectroscopy for  
656 wastewater monitoring: A review, *Water Res.*, 2016, **95**, 205-219.
- 657 52. R. K. Henderson, A. Baker, K. R. Murphy, A. Hambly, R. M. Stuetz and S. J. Khan,  
658 Fluorescence as a potential monitoring tool for recycled water systems: A review, *Water Res.*,  
659 2009, **43**, 863-881.
- 660 53. C. Jacquin, G. Lesage, J. Traber, W. Pronk and M. Heran, Three-dimensional excitation and  
661 emission matrix fluorescence (3DEEM) for quick and pseudo-quantitative determination of  
662 protein- and humic-like substances in full-scale membrane bioreactor (MBR), *Water Res.*,  
663 2017, **118**, 82-92.
- 664 54. W. Chen, P. Westerhoff, J. A. Leenheer and K. Booksh, Fluorescence Excitation–Emission  
665 Matrix Regional Integration to Quantify Spectra for Dissolved Organic Matter, *Environ. Sci.*  
666 *Technol.*, 2003, **37**, 5701-5710.

- 667 55. D. D. Phong and J. Hur, Non-catalytic and catalytic degradation of effluent dissolved organic  
668 matter under UVA-and UVC-irradiation tracked by advanced spectroscopic tools, *Water Res.*,  
669 2016, **105**, 199-208.
- 670 56. R. X. Hao, H. Q. Ren, J. B. Li, Z. Z. Ma, H. W. Wan, X. Y. Zheng and S. Y. Cheng, Use of  
671 three-dimensional excitation and emission matrix fluorescence spectroscopy for predicting the  
672 disinfection by-product formation potential of reclaimed water, *Water Res.*, 2012, **46**, 5765-  
673 5776.
- 674 57. B. Guo, S. D. Snow, B. J. Starr, I. Xagorarakis and V. V. Tarabara, Photocatalytic inactivation  
675 of human adenovirus 40: Effect of dissolved organic matter and prefiltration, *Sep. Purif.*  
676 *Technol.*, 2018, **193**, 193-201.
- 677 58. S. Mozia, Photocatalytic membrane reactors (PMRs) in water and wastewater treatment. A  
678 review, *Sep. Purif. Technol.*, 2010, **73**, 71-91.
- 679 59. X. Zheng, Z. P. Shen, L. Shi, R. Cheng and D. H. Yuan, Photocatalytic Membrane Reactors  
680 (PMRs) in Water Treatment: Configurations and Influencing Factors, *Catalysts*, 2017, **7**, 30.
- 681 60. B. Pernet-coudrier, L. Clouzot, G. Varrault, M.-H. Tusseau-vuillemin, A. Verger and J.-M.  
682 Mouchel, Dissolved organic matter from treated effluent of a major wastewater treatment  
683 plant: Characterization and influence on copper toxicity, *Chemosphere*, 2008, **73**, 593-599.
- 684 61. D. Violleau, H. Essis-Tome, H. Habarou, J. P. Croué and M. Pontié, Fouling studies of a  
685 polyamide nanofiltration membrane by selected natural organic matter: an analytical approach,  
686 *Desalination*, 2005, **173**, 223-238.
- 687 62. X. Zheng, M. T. Khan and J.-P. Croué, Contribution of effluent organic matter (EfOM) to  
688 ultrafiltration (UF) membrane fouling: Isolation, characterization, and fouling effect of EfOM  
689 fractions, *Water Res.*, 2014, **65**, 414-424.
- 690 63. G. R. Aiken, D. M. McKnight, K. A. Thorn and E. M. Thurman, Isolation of hydrophilic  
691 organic acids from water using nonionic macroporous resins, *Org. Geochem.*, 1992, **18**, 567-  
692 573.
- 693 64. J. A. Leenheer, Systematic Approaches to Comprehensive Analyses of Natural Organic  
694 Matter, *Ann. Environ. Sci.*, 2009, **3**.
- 695 65. J. L. Weishaar, G. R. Aiken, B. A. Bergamaschi, M. S. Fram, R. Fujii and K. Mopper,  
696 Evaluation of Specific Ultraviolet Absorbance as an Indicator of the Chemical Composition  
697 and Reactivity of Dissolved Organic Carbon, *Environ. Sci. Technol.*, 2003, **37**, 4702-4708.
- 698 66. C. Goletz, M. Wagner, A. Grübel, W. Schmidt, N. Korf and P. Werner, Standardization of  
699 fluorescence excitation–emission-matrices in aquatic milieu, *Talanta*, 2011, **85**, 650-656.
- 700 67. M. Cho, H. Chung, W. Choi and J. Yoon, Linear correlation between inactivation of *E. coli*  
701 and OH radical concentration in TiO<sub>2</sub> photocatalytic disinfection, *Water Res.*, 2004, **38**, 1069-  
702 1077.
- 703 68. J. R. Bolton and K. G. Linden, Standardization of methods for fluence (UV dose)  
704 determination in bench-scale UV experiments, *ASCE J. Environ. Eng.*, 2003, **129**, 209-215.
- 705 69. M. L. Quaranta, M. D. Mendes and A. A. MacKay, Similarities in effluent organic matter  
706 characteristics from Connecticut wastewater treatment plants, *Water Res.*, 2012, **46**, 284-294.
- 707 70. T. Masuda, S. Nakano and M. Kondo, Rate Constants for the Reactions of OH Radicals with  
708 the Enzyme Proteins as Determined by the p-Nitrosodimethylaniline Method, *Journal of*  
709 *Radiation Research*, 1973, **14**, 339-345.
- 710 71. C. L. Hawkins and M. J. Davies, Generation and propagation of radical reactions on proteins,  
711 *Biochim. Biophys. Acta*, 2001, **1504**, 196-219.
- 712 72. Y. Pi, J. Schumacher and M. Jekel, The Use of para-Chlorobenzoic Acid (pCBA) as an  
713 Ozone/Hydroxyl Radical Probe Compound, *Ozone: Science & Engineering*, 2005, **27**, 431-  
714 436.
- 715 73. I. Michael-Kordatou, C. Michael, X. Duan, X. He, D. D. Dionysiou, M. A. Mills and D. Fatta-  
716 Kassinos, Dissolved effluent organic matter: Characteristics and potential implications in  
717 wastewater treatment and reuse applications, *Water Res.*, 2015, **77**, 213-248.
- 718 74. A. Matilainen, E. T. Gjessing, T. Lahtinen, L. Hed, A. Bhatnagar and M. Sillanpää, An  
719 overview of the methods used in the characterisation of natural organic matter (NOM) in  
720 relation to drinking water treatment, *Chemosphere*, 2011, **83**, 1431-1442.

- 721 75. J. K. Edzwald and J. E. Tobiasson, Enhanced coagulation: Us requirements and a broader view,  
722 *Water Sci. Technol.*, 1999, **40**, 63-70.
- 723 76. M. Drosos, M. J. Ren and F. H. Frimmel, The effect of NOM to TiO<sub>2</sub>: interactions and  
724 photocatalytic behavior, *Appl. Catal. B-Environ.*, 2015, **165**, 328-334.
- 725 77. Y. Sun and J. J. Pignatello, Evidence for a surface dual hole-radical mechanism in the titanium  
726 dioxide photocatalytic oxidation of 2,4-D, *Environ. Sci. Technol.*, 1995, **29**, 2065-2072.
- 727 78. X. Huang, M. Leal and Q. Li, Degradation of natural organic matter by TiO<sub>2</sub> photocatalytic  
728 oxidation and its effect on fouling of low-pressure membranes, *Water Res.*, 2008, **42**, 1142-  
729 1150.
- 730 79. E. Bouhabila, R. Ben Aim and H. Buisson, Fouling characterisation in membrane bioreactors,  
731 *Sep. Purif. Technol.*, 2001, **22-3**, 123-132.
- 732 80. S. L. Gora and S. A. Andrews, Adsorption of natural organic matter and disinfection  
733 byproduct precursors from surface water onto TiO<sub>2</sub> nanoparticles: pH effects, isotherm  
734 modelling and implications for using TiO<sub>2</sub> for drinking water treatment, *Chemosphere*, 2017,  
735 **174**, 363-370.
- 736 81. J. F. Budarz, A. Turolla, A. F. Piasecki, J. Y. Bottero, M. Antonelli and M. R. Wiesner,  
737 Influence of Aqueous Inorganic Anions on the Reactivity of Nanoparticles in TiO<sub>2</sub>  
738 Photocatalysis, *Langmuir*, 2017, **33**, 2770-2779.
- 739 82. C. S. Turchi and D. F. Ollis, Photocatalytic degradation of organic water contaminants:  
740 Mechanisms involving hydroxyl radical attack, *J. Catal.*, 1990, **122**, 178-192.
- 741 83. T. E. Doll and F. H. Frimmel, Photocatalytic degradation of carbamazepine, clofibric acid and  
742 iomeprol with P25 and Hombikat UV100 in the presence of natural organic matter (NOM) and  
743 other organic water constituents, *Water Res.*, 2005, **39**, 403-411.
- 744 84. M. Long, J. Brame, F. Qin, J. Bao, Q. Li and P. J. Alvarez, Phosphate Changes Effect of  
745 Humic Acids on TiO<sub>2</sub> Photocatalysis: From Inhibition to Mitigation of Electron-Hole  
746 Recombination, *Environ. Sci. Technol.*, 2017, **51**, 514-521.
- 747 85. B. J. Starr, V. V. Tarabara, M. Herrera-Robledo, M. Zhou, S. Roualdès and A. Ayral, Coating  
748 porous membranes with a photocatalyst: Comparison of LbL self-assembly and plasma-  
749 enhanced CVD techniques, *J. Membr. Sci.*, 2016, **514**, 340-349.

750